Title

Differential Sources for 2 Neural Signatures of Target Detection: An Electrocorticography Study.

Journal

Cerebral Cortex, 28(1)

ISSN

1047-3211

Authors

Kam, JWY
Szczepanski, SM
Canolty, RT
et al.

Publication Date

2018

DOI

10.1093/cercor/bhw343

Peer reviewed

Cerebral Cortex, January 2018;28: 9–20

doi: 10.1093/cercor/bhw343
Advance Access Publication Date: 22 November 2016
Original Article

ORIGINAL ARTICLE

Differential Sources for 2 Neural Signatures of Target Detection: An Electrocorticography Study

J. W. Y. Kam[1,†], S. M. Szczepanski[1,†], R. T. Canolty[1], A. Flinker[2], K. I. Auguste[3,4], N. E. Crone[5], H. E. Kirsch[6], R. A. Kuperman[7], J. J. Lin[8], J. Parvizi[9,10] and R. T. Knight[1,11]

[1]Helen Wills Neuroscience Institute, University of California, Berkeley, Berkeley, CA 94720, USA, [2]Department of Psychology, New York University, New York, NY 10012, USA, [3]Department of Surgery, Division of Neurological Surgery, Children's Hospital and Research Center, Oakland, CA 94609, USA, [4]Department of Neurological Surgery, University of California, San Francisco, San Francisco, CA 94143, USA, [5]Department of Neurology, Epilepsy Center, Johns Hopkins Medical Institutions, Baltimore, MD 21224, USA, [6]Department of Neurology, Division of Epilepsy and Department of Radiology and Biomedical Imaging, University of California, San Francisco, San Francisco, USA, [7]Department of Neurology, Children's Hospital and Research Center, Oakland, CA 94609, USA, [8]Department of Neurology, University of California, Irvine, Irvine, CA 92697, USA, [9]Laboratory of Behavioral and Cognitive Neurology, Department of Neurology and Neurological Sciences, Stanford University, Stanford, CA 94305, USA, [10]Human Intracranial Cognitive Electrophysiology Program (SHICEP), Stanford University, Stanford, CA 94305, USA and [11]Department of Psychology, University of California, Berkeley, Berkeley, CA 94720, USA

Address correspondence to J. W. Y. Kam or S. M. Szczepanski. Email: kamjulia@gmail.com or sszczepa@berkeley.edu

[†]These authors contributed equally to the manuscript.

Abstract

Electrophysiology and neuroimaging provide conflicting evidence for the neural contributions to target detection. Scalp electroencephalography (EEG) studies localize the P3b event-related potential component mainly to parietal cortex, whereas neuroimaging studies report activations in both frontal and parietal cortices. We addressed this discrepancy by examining the sources that generate the target-detection process using electrocorticography (ECoG). We recorded ECoG activity from cortex in 14 patients undergoing epilepsy monitoring, as they performed an auditory or visual target-detection task. We examined target-related responses in 2 domains: high frequency band (HFB) activity and the P3b. Across tasks, we observed a greater proportion of electrodes that showed target-specific HFB power relative to P3b over frontal cortex, but their proportions over parietal cortex were comparable. Notably, there was minimal overlap in the electrodes that showed target-specific HFB and P3b activity. These results revealed that the target-detection process is characterized by at least 2 different neural markers with distinct cortical distributions. Our findings suggest that separate neural mechanisms are driving the differential patterns of activity observed in scalp EEG and neuroimaging studies, with the P3b reflecting EEG findings and HFB activity reflecting neuroimaging findings, highlighting the notion that target detection is not a unitary phenomenon.

Key words: electrocorticography, high frequency band, neural generators, P3b, target detection

Introduction

Detection of environmental events is essential for carrying out day-to-day activities, and abnormalities in the electrophysiological marker of this cognitive function are observed in numerous neurological and psychiatric disorders (Polich and Herbst 2000). The prominent role of target detection in daily functioning highlights the importance of defining the neural mechanisms and brain regions supporting this core cognitive process. Target detection is indexed by the well-studied P3b event-related potential (ERP) component (Sutton et al. 1965; Duncan-Johnson and Donchin 1977; Pritchard 1981; Donchin and Coles 1988; Linden 2005; Polich 2007). The spatiotemporal dynamics of the scalp P3b marker of target detection are well established with a parietal scalp topography and a peak onset at approximately 300 ms after target occurrence. Functional magnetic resonance imaging (fMRI) has further characterized the spatial distribution of the brain regions with an increased hemodynamic response to target events. However, the electrophysiological and functional neuroimaging literature provide conflicting evidence for the neural regions contributing to target detection.

Neural Contributions to Target Detection: Electrophysiological Evidence

Scalp electroencephalography (EEG) studies attempting to localize the origin of the P3b component generally converge on the parietal cortex across modalities. The most commonly occurring dipoles are located over superior temporal and inferior parietal cortices in auditory target-detection tasks (Mecklinger and Ullsperger 1995; Anderer et al. 1998; Opitz et al. 1999; Mulert et al. 2004) and over both inferior and superior parietal cortices in visual target-detection tasks (Moores et al. 2003; Bledowski et al. 2004). Some of the variability in these studies may stem from theoretical limitations of source reconstruction. A reversible lesion to parietal scalp sites using transcranial magnetic stimulation reduces visual target-detection ability, providing behavioral support for the source localization studies (Muggleton et al. 2008).

Human lesion studies offer compelling and causal evidence for the origin of the P3b component. Convergent evidence from these studies suggests that the parietal cortex, especially the temporo–parietal junction (TPJ), is necessary for successful target detection and P3b generation in the auditory modality (Knight et al. 1989; Verleger et al. 1994). In the visual modality, lesion studies examining the visual P3b response suggest that the TPJ is involved, but plays a less critical role in the detection of visual targets (Verleger et al. 1994; Knight 1997). Rather, lesions to a more rostral part of the parietal cortex result in significant decreases in the visual P3b response (Verleger et al. 1994). Taken together, the neural source for both the auditory and visual P3b appears to lie mainly in posterior cortices.

Neural Contributions to Target Detection: Neuroimaging Evidence

Electrophysiological and lesion studies converge on parietal cortex as the main neural generator of the target-related P3b component across modalities. In contrast, fMRI studies have identified a network of frontal and parietal areas that are consistently activated during the detection of auditory (Linden et al. 1999; Mulert et al. 2004) or visual targets (McCarthy and Wood 1987; Linden et al. 1999). In particular, target-related activations have been reported in multiple parietal regions, including the supramarginal gyrus (Linden et al. 1999) and TPJ (Mulert et al. 2004), confirming previous EEG and lesion results. Further, fMRI studies have reported blood oxygen level-dependent (BOLD) signal increases in several frontal regions (McCarthy et al. 1989; Linden et al. 1999; Downar et al. 2001; Ardekani et al. 2002; Horovitz et al. 2002; Mulert et al. 2004) during oddball tasks, with the most commonly reported region centered in the inferior frontal gyrus (Mulert et al. 2004; Brázdil et al. 2005). This work supports Corbetta and Shulman's (2002) proposal that the inferior frontal gyrus is involved in target detection and is specifically important for re-orienting to salient, behaviorally relevant targets.

Electrocorticography and High Frequency Band Activity

In summary, scalp EEG studies localize the origin of the P3b component to the parietal cortex, whereas fMRI studies localize the target-related activations to both frontal and parietal cortices. Our study addresses this discrepancy between EEG/lesion and fMRI findings by examining the sources that give rise to the target-detection process using electrocorticography (ECoG). The ECoG signal has millisecond temporal resolution, similar to scalp EEG, and subcentimeter spatial resolution, similar to fMRI, rendering it an excellent tool for examining the neural regions giving rise to cognitive functions.

One feature of the ECoG signal that is particularly relevant to the current study is high frequency band (HFB) activity, which is characterized as broadband activity measured between 70 and 250 Hz or higher on the cortical surface. HFB activity has been linked to the BOLD signal of fMRI in previous studies (Logothetis et al. 2001; Nir et al. 2007), as well as neuronal firing rate (Miller 2010; Ray and Maunsell, 2011; Keller et al., 2016). Past studies using intracranial recordings to examine target detection have reported HFB increases in response to targets relative to nontargets (Bansal et al. 2014; Nourski et al. 2014). Although these studies characterized the electrophysiological correlates of target detection, either they selectively focused on the superior temporal gyrus (Nourski et al. 2014) or they used a restrictive frequency range (70–100 Hz) to define the broadband HFB signal (Bansal et al. 2014), and neither study addressed the discrepancy between the EEG/lesion and fMRI literature.

We recorded ECoG activity from 14 patients undergoing presurgical monitoring for intractable epilepsy as they performed a target-detection task in either the auditory or visual modality, and examined the target-related response in 2 domains: HFB (69–145 Hz) and the P3b ERP response. We focused specifically on the frontal cortex and parietal cortex, as they are the most commonly occurring regions of target-related activation across modalities and methodologies. We hypothesized that the discrepancy in the EEG and fMRI literature originates in the activity of 2 distinct neural correlates of target detection, with the reported P3b reflecting findings from the scalp EEG literature and the reported HFB activity reflecting the BOLD signal findings from the fMRI literature. In particular, we predicted more HFB relative to P3b activity over the frontal cortex, whereas the parietal cortex would show comparable amounts of HFB and P3b activity.

Materials and Methods

Patients

Recordings were obtained from patients undergoing presurgical monitoring for intractable epilepsy. Six patients (S1–S6; mean age = 35.5 years, age range: 21–45 years, 5 females) participated in the auditory experiment and eight patients (S7–S14; mean

age = 30.6 years, age range: 18–52 years, 3 females) participated in the visual experiment. All patients provided written informed consent, and the Institutional Review Board (IRB) at each university approved the research protocol.

Target Detection Tasks

Auditory Tasks

Auditory stimuli were recorded from a female native English speaker, and presented via 2 speakers using custom scripts written in MATLAB. Patients performed 1 of 2 auditory target-detection tasks, in which they were instructed to tap a microphone in response to the target. Four patients performed the "word" task (described in detail in Canolty et al. 2007), and two patients performed the "phoneme" task (described in detail in Flinker et al. 2010).

In the "word" task, proper names served as target stimuli (9.5% occurrence rate) among action verbs (45.25% occurrence rate) and acoustically matched but unintelligible nonwords (45.25% occurrence rate). Each stimulus lasted 637ms, and was presented in a randomized order with an interstimulus interval (ISI) of 1063 ± 100 ms. Only action verbs were considered as the nontarget stimuli in the current study to ensure that the semantic properties of target and nontarget stimuli were similar. All trials were designated by response type (hits, misses, correct rejections, and false alarms). An average of 40 targets and 192 action verb nontargets were presented during the task. All target and nontarget stimuli to which subjects correctly responded (designated as hits and correct rejections, respectively) were included in subsequent analyses. There was an exception with S1, whose behavioral data were missing. Given the overall high accuracy rate across subjects on this task (as reported in the Results section), we included all target and nontarget trials for S1 in subsequent analyses.

In the "phoneme" task, the target stimulus was the "oo" vowel sound (11% occurrence rate; 37.5 trials on average), which was played among 8 other English phonemes (89% occurrence rate; 300 trials on average). Stimulus duration varied in length (215–350 ms), and they were presented in a pseudorandom manner, with a jittered ISI of 2s ± 250 ms. Only targets and nontargets to which subjects correctly responded (designated as hits and correct rejections, respectively) were included in subsequent analyses.

Visual Task

Visual displays were generated on a Dell Precision M4600 laptop (Dell, Inc.) using EPrime software (Psychology Software Tools, Inc.). Subjects were seated 50–60 cm from the computer screen as they performed a visual target-detection task: the Starry Night Test (described in detail in Szczepanski et al. 2014). During the task, they attended either to the left visual field (LVF) or to the right visual field (RVF) and fixated on a cross in the middle of the screen during each trial. On each trial, subjects covertly attended to the instructed visual field (cued by a central arrow) and pressed a button when a blue square stimulus (6.5 mm^2 in size) appeared. Stimulus onset was jittered from 1000 to 2000 ms relative to trial/cue onset. Each stimulus that appeared in the cued/attended visual field remained on the screen until the subject responded, at which point the screen turned black during a 500-ms intertrial interval (ITI). At the end of the ITI, a new trial began with a new cue appearance. Subjects withheld responses to stimuli that appeared in the uncued/unattended field. An unattended stimulus remained on the screen for 2000 ms, followed by a 500-ms ITI. The blue square stimuli appeared ~62% on the cued/attended side (the target trials) and ~38% on the uncued/unattended side (the nontarget trials). All blue square stimuli appeared on a dynamic background of red circle distracters (each 4 mm in diameter), which could turn on or off. LVF and RVF cued conditions were blocked and the order of blocks was counterbalanced between subjects.

All analyzed trials were time-locked to the appearance of each blue square stimulus and were classified as either a target (i.e., the stimulus appeared in cued visual field) or a nontarget (i.e., the stimulus appeared in the uncued visual field). All trials were designated by response type (hits, misses, correct rejections, and false alarms). Only targets and nontargets to which subjects correctly responded (designated as hits and correct rejections, respectively) were included in subsequent analyses. A mean of 138.5 target and 85.4 nontarget trials were presented during the task.

Behavioral Measures

For both the auditory and visual tasks, reaction times (RTs) for target trials, *d*-prime (*d'*), and accuracy rates (i.e., hits and correct rejections) were computed for each subject. Paired-samples *t*-tests were then used to analyze the behavioral results.

Electrode Placement and Localization

Figure 1 shows the overlap of electrodes from all patients from the 1) auditory experiment and 2) visual experiment. The placement of electrodes was determined solely on clinical grounds and varied across individuals. In the auditory experiment, patients were implanted with a 64-channel grid of subdural electrodes (with 1 cm spacing) placed on the cortical surface over lateral frontal, parietal, and temporal cortices in the right hemisphere (RH) and left hemisphere (LH). In the visual experiment, subjects were implanted with 74–128 subdural electrodes

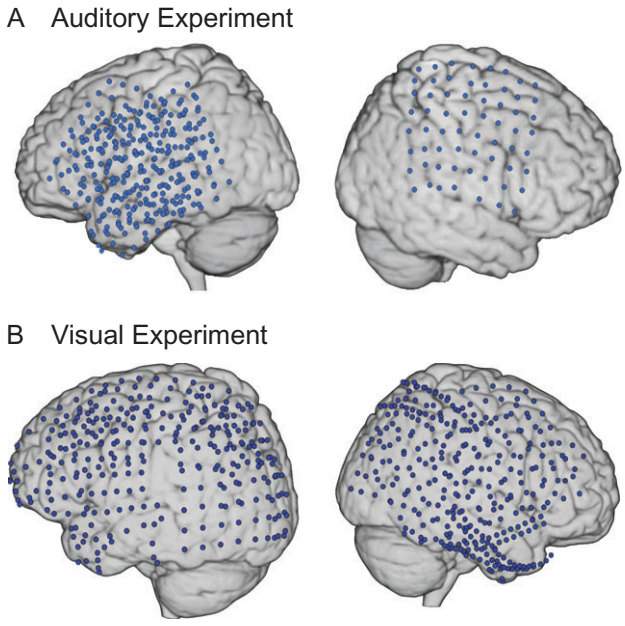

Figure 1. Composite map of implanted grids. Electrodes across patients from the (A) auditory experiment (n = 6) and (B) visual experiment (n = 8) are displayed on a standard MNI template brain.

on a grid or strip (with 1 cm spacing), covering extensive portions of lateral and medial frontal, parietal, occipital, and temporal cortices in the RH and LH.

A structural magnetic resonance (MR) image was acquired for each patient prior to implantation. Postimplantation computed tomography (CT) scans were obtained and coregistered to the preoperative structural MR images. Two patients (S3, S4) did not have a CT scan, so electrode localization was based on the intraoperative digital photographs, which was approved by a neurologist. Each patient's brain was then transformed into Montreal Neurological Institute (MNI) space to allow for electrode visualization and localization on the 3D cortical surface with corresponding MNI coordinates. The aforementioned steps were performed using Brain Extraction Tool (http://www.fmrib.ox.ac.uk/analysis/research/bet/), MRIcro (http://www.sph.sc.edu/comd/rorden/mricro.html), SPM8 (http://www.fil.ion.ucl.ac.uk/spm/software/spm2) and MATLAB, and BioImage suite (http://www.bioimagesuite.org). Details of the electrode localization process have been described elsewhere (Canolty et al. 2007; Flinker et al. 2010; Szczepanski et al. 2014).

ECoG Data Acquisition and Preprocessing

Electrophysiological data were acquired using a 128-channel Nihon Kohden recording system (Nihon Kohden Corporation) at Children's Hospital (1000 Hz digitization) and at the University of California, Irvine (5000 Hz digitization), a 128-channel Stellate Harmonie recording system (Natus Medical, Inc.; 1000 Hz digitization) at Johns Hopkins, a 128-channel Tucker Davis Technologies recording system at Stanford University (3052 Hz digitization), and a 256-channel Tucker Davis Technologies recording system at the University of California, San Francisco (2003 Hz digitization). Data were recorded using a subdural electrode reference and an extracranial ground.

A neurologist manually inspected all ECoG channels to identify those with interictal or ictal epileptiform activity and artifacts. Channels and epochs contaminated by epileptiform activity or abnormal signal (e.g., poor contact, excess drift, and high frequency noise) and those located over tissue that was later resected were removed from further analyses. Data processing was performed using custom functions written in MATLAB and the EEGLAB toolbox. Raw, continuous data were down-sampled to 1000 Hz, filtered with a 60-Hz notch filter when necessary, and rereferenced to a common average reference (i.e., mean of nonepileptic and artifact-free channels). Single channels of these ECoG data are referred to as "raw signal" hereafter.

HFB Analyses

The raw ECoG signal was filtered in each frequency range using a frequency domain Gaussian filter (similar to the one described by Canolty et al. 2007). An input signal X was transformed to the frequency domain signal X_f using an N-point *fft* (where N is defined by the number of points in the time series X). In the frequency domain, a Gaussian filter was constructed (for both the positive and negative frequencies) and multiplied with the signal X_f. The subsequent signal was transformed back to the time domain using an inverse *fft*. The Hilbert Transform was then applied to these filtered signals to create a complex-valued analytic time series. Squaring the modulus (element-wise) of the complex-valued analytic time series created the instantaneous power time series.

Event-related spectral perturbations (ERSPs) were first calculated for each electrode. Forty-four logarithmically equally spaced frequency bands were created from 1 to 250 Hz. The instantaneous power time series was calculated for each frequency band and ERSPs were created for each condition by averaging the power time series across all trials from that condition (−200 to 800 ms poststimulus). For the condition with more trials, ERSPs were created from an average of 100 bootstrapped subsamples. The rationale and procedures of bootstrapping are described in detail below. For data normalization, a bootstrapped distribution of baseline values was created by randomly choosing N (i.e., number trials/condition) baseline values (−200 to 0 ms) and averaging across these values (for 1000 iterations). The ERSP was normalized (per frequency) by subtracting the mean of the baseline distribution and dividing by the standard deviation (SD) of the baseline distribution, and was subsequently represented as z-scores. The red and blue portions of each graph in Figure 2 are at least ±3.3 z-scores ($P < 0.001$), respectively, from the mean of the baseline.

Given that the HFB signal-to-noise ratio increases with trial numbers, we performed bootstrapping with replacement such that nontarget trials were randomly sampled 100 times to match the number of target trials in the auditory tasks. We then averaged across the 100 random subsamples to derive representative HFB z-score values for every millisecond time point within the 800-ms poststimulus time window for nontarget trials. In the visual task, this bootstrapping procedure was performed on target trials, as the target condition contained more trials than the nontarget condition. The matched trial numbers ensured that conditional effects found in HFB power were not simply due to differences in signal-to-noise ratio resulting from a mismatched number of trials across conditions. These bootstrapped mean z-scores for the matched condition (nontarget trials for the auditory task and target trials for the visual task) were then used for all subsequent analyses as well as ERSPs as presented in Figure 2.

Electrodes were counted as having significant HFB increases if the average HFB power (69–145 Hz) z-score value across target trials was above the z-score cutoff at 3.3 ($P < 0.001$) for a minimum of 50 consecutive milliseconds anywhere within the time window of 0–800 ms following stimulus onset. Next, this subset of electrodes showing significant HFB responses to targets relative to baseline was examined for target and nontarget conditional differences using permutation testing. For each of the 500 permutations, the condition labels of the HFB z-score time series were shuffled, and a surrogate HFB difference time series was derived by subtracting the shuffled HFB "nontarget" z-scores from the shuffled HFB "target" z-scores at each time point across the 800-ms poststimulus time window. The surrogate HFB difference z-score time series were then compared with the observed HFB difference z-score time series, both of which were binned into consecutive, nonoverlapping 10-ms time windows.

We examined whether the surrogate HFB difference z-score time series was greater than the observed HFB difference z-score time series for a minimum of 100 consecutive ms anywhere within the time window of 0–800 ms following stimulus onset for each permutation. This criterion results in a binary outcome for each permutation: 1) there were no conditional differences (i.e., the surrogate difference z-score time series was not greater than the observed difference z-score time series for over 100 consecutive ms) or 2) there were conditional differences (i.e., the surrogate difference z-score time series was greater than the observed difference z-score time series for

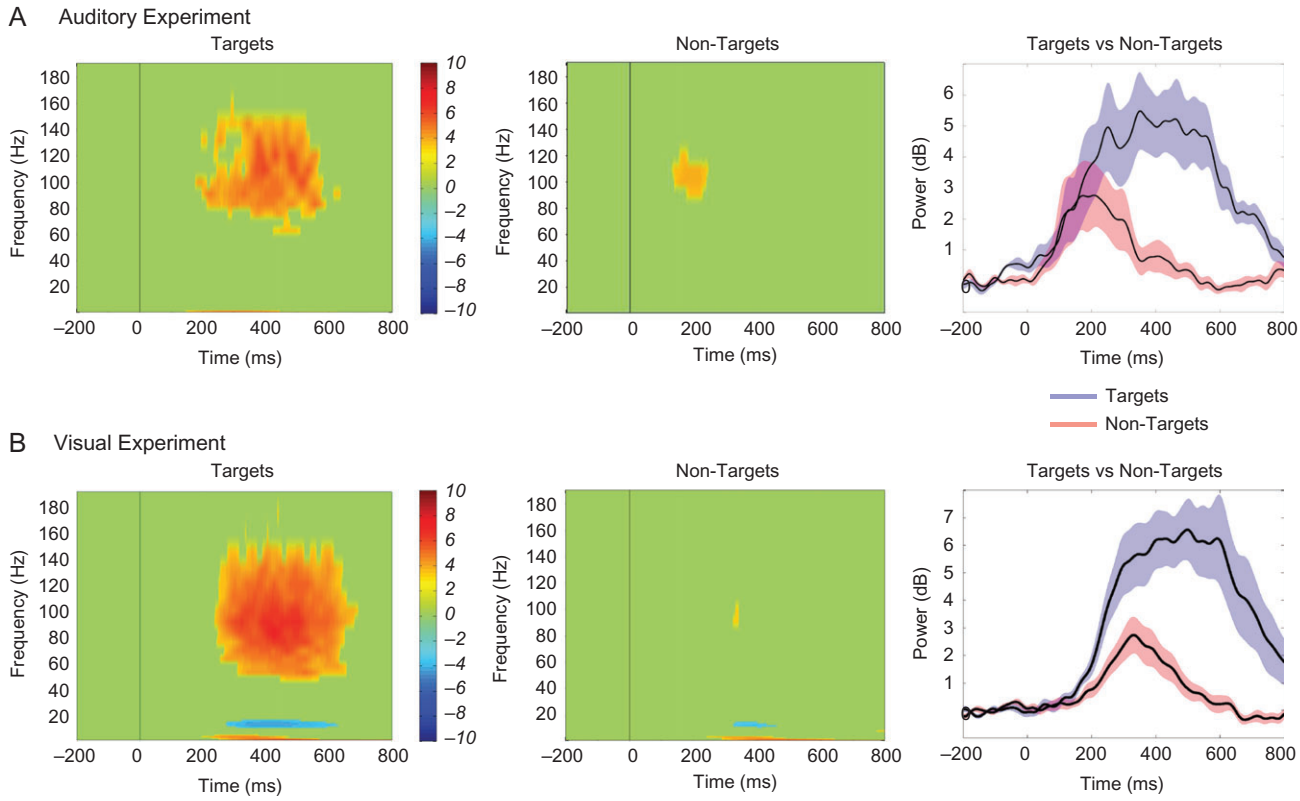

Figure 2. ERSPs of task conditions for each experiment. The ERSP of target-related (left panel) and nontarget-related activity (middle panel) represented as z-score values and averaged across electrodes showing target-specific effects are shown for (*A*) a representative subject (S5) in the auditory experiment and (*B*) a representative subject (S14) in the visual experiment. The HFB power (69–145 Hz) time series (right panel) averaged across those same electrodes for targets (in blue) and nontargets (in red) and for each subject are also shown separately for each experiment.

over 100 consecutive ms). Across the 500 permutations, we computed the proportion of times these permutations based on randomly shuffled data led to conditional differences (i.e., the second outcome). This proportion reflects the *P* value, which is the probability that a conditional effect was observed by chance. We then compared the *P* value with the critical alpha level we set at 0.05, which equates to 25 permutations out of 500. Therefore, if this proportion was below 0.05 in a given electrode, we concluded that the target and nontarget conditions were significantly different in that electrode. If the number of random permutations resulting in conditional differences was less than 25, then that electrode was considered to show true significant conditional differences, and is referred to as a "target-specific" electrode hereafter.

All electrodes showing clear motor activity (as indicated by single-trial HFB activity sorted according to response time) were excluded from all HFB analyses and were not reported in the current study. This assured that the observed conditional differences were driven by target-related cognitive-level processing, rather than motor responses to the targets. See Supplementary Figure 1 for examples of electrodes with motor activity as indicated by single-trial traces of HFB power.

ERP Analyses

In order to compute the P3b, the raw signal for each electrode was bandpass filtered between 0.1 and 8 Hz. Each trial was normalized to its own baseline (by subtracting the mean of the 200-ms preceding each trial from each poststimulus time point), and trials were averaged within each condition of interest in order to create separate ERP waveforms for target and nontarget conditions. Trials that qualified as outliers, as described below, were excluded from subsequent analyses and were not included in grand average ERP waveforms. For each electrode and condition, if the difference between the maximum and minimum amplitude in the poststimulus window (0–700 ms) for a specific trial exceeded 5 SDs above the average amplitude across trials, then the trial was considered an outlier (see Bansal et al. 2014 for a similar approach). An average of 7.52% and 0.44% of outlier trials across participants were removed in the auditory and visual tasks, respectively. The number of trials removed did not differ between target and nontarget conditions (auditory, $P = 0.19$; visual, $P = 0.08$). Moreover, the same electrodes that showed clear motor activity, based on single-trial HFB activity, were also excluded from all ERP analyses.

We only considered an electrode for subsequent analyses if its ERP waveform averaged across target trials significantly differed from baseline for a consecutive 100-ms time window between 200 and 600 ms following target onset (see Engell and McCarthy 2011 for a similar approach). We binned the data in the target condition following stimulus onset (0–700 ms) into consecutive, nonoverlapping 10 ms time windows and used paired-sample *t*-tests to test the mean amplitude in each of these bins to the mean amplitude of the baseline (–200 to 0 ms). A false-discovery rate (FDR) procedure was used to correct for multiple comparisons (Benjamini and Hochberg 1995). An electrode with 100 ms of consecutive time points (i.e., 10

consecutive time bins) that was significantly higher than baseline between 200 and 600 ms poststimulus onset was considered to have a significant P3b component. This approach allowed us to objectively identify the presence of the P3b in the target condition, by restricting the onset of the response (i.e., 200 ms), the time corresponding to the peak voltage, and the offset of the response (i.e., 600 ms).

Electrodes that fulfilled the above criteria were then tested for target versus nontarget conditional differences using the peak-mean amplitude procedure (Knight et al. 1989). Specifically, the maximal positive voltage between 200 and 500 ms following target onset was first identified and the mean amplitude between 100 ms before and after this peak was derived. For each electrode, the P3b in the target and nontarget conditions was quantified separately using the peak-mean amplitude measure and then compared using a paired samples *t*-test, from which the observed *t*-value was derived. Permutation testing was performed to determine the significance between conditions. For each of the 500 permutations, we shuffled the condition labels of the P3b peak-mean amplitudes, and computed the *t*-value using a paired samples *t*-test on the shuffled P3b values for the surrogate "nontarget" trials and "target" trials. Across the 500 permutations, we calculated the proportion of times these permutations yielded a surrogate *t*-value exceeding the observed *t*-value. According to the standard approach (Maris and Oostenveld, 2007), this proportion reflects the *P* value. If the *P* value was below our predetermined critical alpha level at 0.05 (i.e., 25 permutations), then that electrode was considered a "target-specific" electrode.

We performed this complete analysis for the visual experiment (see Results section) and the auditory experiment (see Supplementary Materials). However, the approach to select electrodes showing target-locked responses for subsequent analyses was not ideal for conditions with a small number of trials, as was the case with the target condition in both auditory tasks. A robust baseline period is crucial to allow for sufficient power to detect significant differences between the stimulus-locked response and baseline activity. The low trial numbers in the target condition in the auditory tasks yielded a more variable baseline, which lead to decreased power to detect significant differences (Handy 2004). Accordingly, for the auditory tasks, instead of first testing for significant differences between the response period and baseline activity in the target condition, we directly tested for target versus nontarget conditional differences. This was a useful method to overcome the noisy baseline issue, since noise common to both the target and nontarget conditions was cancelled out in this comparison. Notably, this is a method commonly used in scalp ERP analyses, as examination of conditional differences allows for a functional interpretation of an ERP component (Luck 2005).

Given the fewer number of trials in the auditory task relative to the visual task, we examined the likelihood of detecting an effect if the effect actually exists. To accomplish this, we performed a post hoc power analysis, in which an input of the sample size and effect size yielded the "achieved" power. Since significant conditional differences in the P3b were tested separately for each electrode, the sample size in this context reflects the number of trials. We computed power separately for the auditory and visual tasks, as the mean number of target and nontarget trials differed, which could influence power. Specifically, there was a mean of 139 target trials and 85 nontarget trials in the visual task, and a mean of 35 target trials and 222 nontarget trials in the auditory task. We set the effect size as 0.7362 based on one previous intracranial study examining ERPs that reported relevant values critical to computing an effect size (Clarke et al., 1999). This yielded power values of 0.9809 for the auditory task and 0.9996 for the visual task. We also computed power separately for each subject based on each subject's respective target and nontarget trial numbers in order to ensure power was sufficient to detect conditional differences at the individual subject level. For the auditory task, the power for each of the 6 subjects ranged from 0.9553 to 0.9883, whereas for the visual task, the power for each of the 8 subjects ranged from 0.9985 to 0.9999. The higher power values for the visual task reflect the higher number of target trials and more comparable trial numbers across conditions. We note that the power values appear to be high. This is in part due to the high effect size reported in Clarke et al. (1999), which is one of the rare intracranial ERP studies that reported the statistical values critical for computing effect sizes for individual electrodes.

For the target-specific P3 electrodes, we performed an exploratory analysis to examine the relationship between low frequency power and the P3b. Supplementary Figure 2 shows the ERSP featuring power in a low frequency range (1–50 Hz) averaged across all target-specific P3 electrodes for a representative subject in the auditory and visual tasks. We report the methods and results for this figure in detail in the Supplementary Materials.

Spatial Distribution of HFB and P3b

We examined the distribution of HFB and P3b responses across the cortex by computing the proportion of electrodes that showed significant target-specific (i.e., increases in target relative to nontarget) HFB and P3b activity within the frontal cortex and parietal cortex. For example, the number of frontal electrodes showing significant conditional differences in HFB activity was divided by the total number of electrodes over frontal cortex. The Wilcoxon signed-rank test (Wilcoxon 1945) was then used to compare the proportion of electrodes with HFB versus P3b responses in frontal and parietal cortices separately. As there was no significant main effect of modality on the proportion of HFB and P3b electrodes across areas ($U = 9.00$, $P = 0.06$), we included all subjects from both experiments in the aforementioned analyses, with the exception of one subject in the visual experiment (S8), who did not have frontal coverage. This subject was only excluded from analyses involving the frontal cortex.

In an exploratory analysis, we averaged the HFB and P3b responses within the poststimulus time window and correlated them across trials to examine the extent to which the activity of these 2 neural markers of target detection fluctuated together. The methods are described in detail in the Supplementary Materials.

Results

Behavioral Performance

For the auditory experiment, the mean RT to target stimuli in the "word" task was 1237 ± 252 ms (mean ± standard error of the mean) and accuracy rate was at ceiling (d' = 7.59 ± 4.12; hits = 95.00 ± 2.50%, correct rejections = 99.74 ± 0.26%). Behavioral data from one patient (S1) were missing, thus the aforementioned behavioral performance reflected the average of the remaining 3 patients. For the "phoneme" task, the mean RT across the 2 patients was 613 ± 342 ms, and accuracy rate was high (d' = 6.63 ± 1.88; hits = 90.00 ± 10.00%, correct rejections = 97.55 ± 0%). In the visual experiment, the mean RT in response to targets was 601 ± 29 ms and accuracy was also

high (d' = 5.03 ± 0.68; hits = 97.21 ± 1.13%, correct rejections = 98.18 ± 0.38%).

HFB Activity

We first determined which electrodes showed statistically significant HFB responses in the target condition relative to baseline (z-score > 3.3, $P < 0.001$) to assess the spatial distribution of HFB activity. Among those electrodes, HFB activity in the target and nontarget conditions was then compared using permutation testing.

Figure 2A shows the ERSP of the target-related activity averaged across all electrodes that showed significant conditional effects (left panel), the ERSP of the nontarget-related activity averaged across those same electrodes (middle panel), and the HFB power (69–145 Hz) time series for each condition averaged across all electrodes that showed significant conditional effects (right panel) for a single representative subject (S5) who performed the auditory experiment. Across all subjects in the auditory experiment (n = 6), a total number of 303 electrodes were analyzed and 46 showed significantly increased HFB responses to the target stimuli relative to baseline in frontal and parietal cortices. Among those, there was a significant increase in HFB activity in the target compared with the nontarget condition in 32 electrodes. As reported in Table 1, these "target-specific" electrodes comprised 19.51% of all electrodes over the frontal cortex and 12.12% of electrodes over the parietal cortex that were included in the analysis.

Across all subjects in the visual experiment (n = 8), 55 electrodes out of a total number of 720 electrodes analyzed showed significant increases in HFB activity in the target condition compared with baseline across frontal and parietal cortices. HFB responses were significantly greater for the targets relative to the nontargets in 25 of these electrodes. Across all electrodes included in the analysis, 3.59% over frontal cortex and 9.83% over parietal cortex showed target-specific HFB activity, as shown in Table 1. Figure 2B shows the ERSP of the target-related activity averaged across all electrodes that showed significant conditional effects (left panel), the ERSP of the nontarget-related activity averaged across those same electrodes (middle panel), and the power (69–145 Hz) time series for each condition averaged across all electrodes that showed significant conditional effects (right panel) for a single representative subject (S14) who performed the visual experiment.

Table 1 Total number of electrodes showing significant target versus nontarget conditional effects in HFB activity and P3b response computed across subjects for each experiment separately is reported as a function of brain region (frontal vs. parietal)

	Auditory (n = 6)	Visual (n = 8)
Frontal		
HFB		
Target only	33	15
Conditional effect	24	7
P3b		
Target only	—	7
Conditional effect	11	1
Total electrodes	123	195
Parietal		
HFB		
Target only	13	40
Conditional effect	8	18
P3b		
Target only	—	35
Conditional effect	4	10
Total electrodes	66	183

Note: For the auditory tasks, we directly tested for target versus nontarget conditional differences in the P3b (as described in the Materials and Methods section). Therefore, only electrodes showing the conditional effect are reported. The total number of electrodes showing significant increases within the target condition only (i.e. target response period compared with baseline period referred to as "Target Only") is reported where applicable. The total number of electrodes analyzed across subjects as a function of brain area is also reported for each experiment.

P3b ERP

We then assessed the spatial distribution and the target specificity of the P3b response. Figure 3 illustrates the stimulus-locked ERP waveforms for individual electrodes within subjects, averaged across electrodes for 2 representative subjects, and averaged across all subjects for each of the 2 experiments.

For the auditory experiment, we directly tested for conditional differences using permutation tests in the P3b response due to small trial numbers (see Materials and Methods section for a detailed explanation). Out of 303 electrodes analyzed, 15 electrodes across frontal and parietal cortices showed significant target-specific increases in P3b amplitude (target vs. nontarget conditional differences in peak-mean amplitude). Figure 3A shows the location and activity of several individual electrodes that showed significant P3b conditional differences for a representative subject (S5; left panel), the target and nontarget ERPs averaged across all electrodes with significant conditional effects for the same representative subject (middle panel), and the average ERP across all 6 subjects (right panel) who performed the auditory experiment. As reported in Table 1, 8.94% of electrodes over frontal cortex and 6.06% over parietal cortex showed these target-specific increases across all electrodes included in the analysis.

For the visual experiment, we first identified electrodes that showed significantly larger P3b components in response to the target stimuli relative to baseline ($P < 0.05$, FDR corrected, for 100 consecutive ms). Forty-two electrodes across frontal and parietal cortices, out of the total 720 electrodes that were analyzed, showed significantly greater target P3b activity during the poststimulus period compared with baseline. Out of these 42 electrodes, 11 showed significant target-specific effects (target vs. nontarget conditional differences in peak-mean amplitude). Figure 3B shows target and nontarget ERPs for several representative electrodes with significant target-specific activity for a representative subject (S14; left panel), averaged across all significant electrodes in the same subject (middle panel), and averaged across all 8 subjects (right panel) who performed the visual experiment. Across all electrodes included in the analysis, 0.51% over frontal cortex and 5.46% over parietal cortex showed target-specific P3b responses, as shown in Table 1.

When inspecting ERP waveforms of individual electrodes in individual subjects, we found a range of distinct morphologies and onset times of the P3b target-detection response over focal locations on the cortex, similar to Halgren et al. (1995a). Examples of the various P3b morphologies that were revealed across individual electrodes are provided for the 2 example subjects, as presented in Figure 3 (left panel). The diversity of the ERP responses in individual electrodes is also reflected in the P3b responses averaged across electrodes for each of these subjects. For example, inspection of the waveforms of the 2 example subjects in Figure 3 (middle panel) suggests that S5 (in

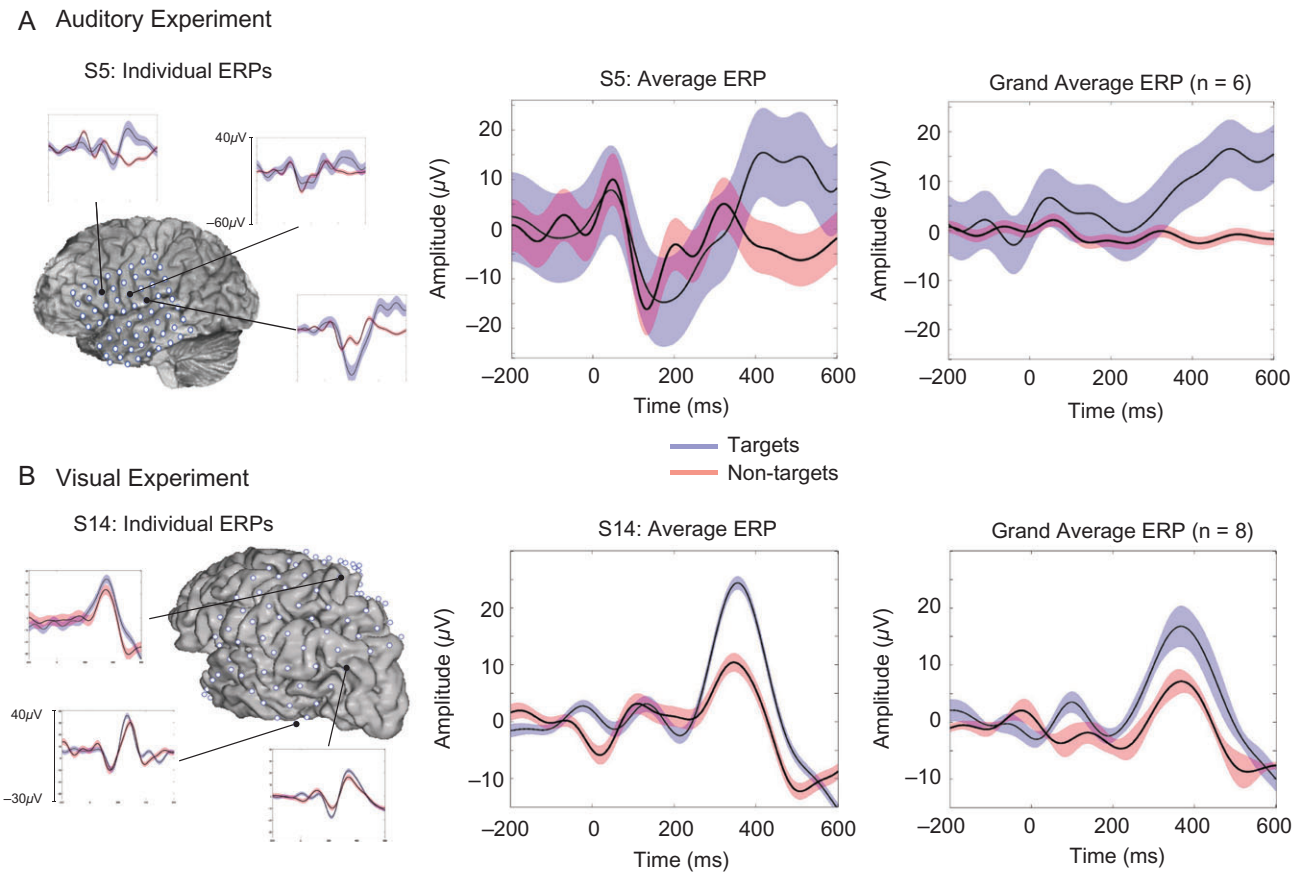

Figure 3. ERP waveforms of task conditions for each experiment. The left column shows the location and ERP waveforms for targets (blue) and nontargets (red) in several example electrodes showing significant target-specific effects for one representative subject in both the (*A*) auditory experiment (S5) and (*B*) visual experiment (S14). In the middle column, the target and nontarget ERP waveforms averaged across all electrodes with significant target-specific effects are shown for the same representative subject for each experiment. The grand average ERP waveforms across all electrodes showing target-specific effects for all subjects for each experiment are shown on the right.

Fig. 3A) shows a wider average P3b with peak onset around 400 ms, whereas S14 (in Fig. 3B) has a narrower average P3b that peaked around 350 ms. Further, the P3b responses averaged across all subjects separately for frontal and parietal electrodes for each of the 2 experiments, as shown in Supplementary Figure 3, highlight the differences in morphology of the P3b waveform as a function of electrode location. Despite the diversity in P3b waveforms across electrodes and subjects, Figure 3 (right panel) illustrates that the greater the number of electrodes included in the grand average ERP waveform, the more the P3b component resembles the stereotypical P3b response observed in scalp EEG. We return to this point in the Discussion section.

Spatial Distribution of HFB and P3b

In order to facilitate the comparison between the spatial distributions of these 2 neural signatures of target detection, we highlighted the electrodes showing target-specific HFB and P3b activity on each individual subject's brain for the auditory experiment and the visual experiment, as shown in Figures 4 and 5, respectively. Visual inspection of the HFB and P3b distributions in each subject in both figures suggests that more target-specific HFB electrodes, relative to target-specific P3b electrodes, are located in the frontal cortex. To directly examine this, we ran Wilcoxon signed-rank tests to compare the proportion of HFB versus P3b electrodes in frontal and parietal cortices across subjects from both experiments. The proportion of electrodes in frontal cortex showing HFB target-specific activity ($M = 0.130$, $SD = 0.100$) was higher than the proportion of electrodes in frontal cortex showing P3b target-specific activity ($M = 0.042$, $SD = 0.068$; $z = -2.67$, $P = 0.008$). In contrast, the proportion of electrodes with HFB target-specific activity in parietal cortex ($M = 0.108$, $SD = 0.073$) did not differ from the proportion of electrodes with P3b target-specific activity in parietal cortex ($M = 0.050$, $SD = 0.077$; $z = -1.61$, $P = 0.108$).

We performed an exploratory analysis to examine the relationship between HFB and P3b across trials. Only a small number of electrodes yielded significant correlations between the HFB and P3b responses. These results are reported in the Supplementary Materials and Supplementary Table 1.

Discussion

We examined the spatial distribution of the target-specific HFB activity and the P3b ERP in 14 epileptic patients during visual and auditory target detection. We found enhanced HFB compared with P3b activity in frontal cortex and equivalent HFB and P3b activity in parietal cortex. Our results suggest that the discrepancy in the spatial distribution of the target response activity between the EEG and fMRI literature is a consequence of these distinct neural correlates contributing to the observed electrophysiological and functional neuroimaging markers.

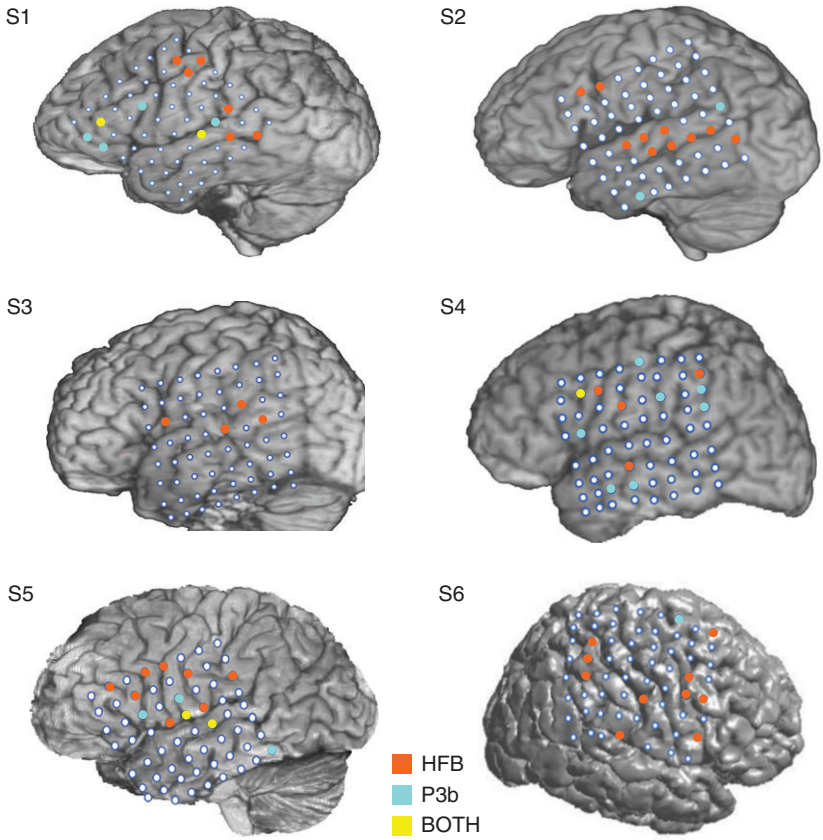

Figure 4. Locations of HFB and P3bs in auditory experiment. The location of electrodes showing target-specific HFB (orange-colored markers), P3b activity (cyan-colored markers), and those electrodes showing both (yellow-colored markers) are presented on each individual subject's brain for the auditory experiment.

Specifically, the parietal ECoG response, which is proposed to be generated by postsynaptic activity, is associated with the P3b scalp ERPs, whereas the HFB response correlated with cortical single unit activity is linked to the frontal and parietal target-elicited BOLD response.

Mechanisms of HFB and P3b in Target Detection

Our findings indicate that target detection activates a distributed network of regions, manifested as 2 neural markers reflecting distinct neural mechanisms. We observed cortical ERPs, possibly generated by postsynaptic potentials on the dendrites of synchronously active neurons (Freeman 2000; Bressler 2002), as well as HFB activity, which has been linked to spiking activity in local neuronal populations (Cardin et al. 2009; Ray and Maunsell, 2011) and the fMRI BOLD response (Logothetis et al. 2001; Nir et al. 2007). Thus, one parsimonious explanation of the inconsistent findings between the EEG/lesion and neuroimaging literature is that the different methods are measuring different neural mechanisms tied to target detection. Scalp EEG studies measure the ERP response over parietal cortex that reflects the observed ECoG P3b, while neuroimaging studies measure the BOLD response that reflects the observed HFB activity over frontal and parietal cortices. It is plausible that the parietal cortex is necessary for the target-detection process, as it has been implicated across sensory modalities and causal methodologies. In contrast, the frontal cortex may play more of a modulatory role of the target-detection response, depending on task demands, behavioral relevance and attention to task. In particular, lesion studies have shown that frontal lesions impair the utilization of contextual information during target detection (Fogelson et al. 2009). These findings suggest differential roles of the frontal and parietal cortices in target detection, with the parietal cortex involved in target processing, while the frontal cortex is important for extracting the contextual and behavioral relevance of the target.

Distributed Neural Generators of Target Detection

There is mixed evidence from source localization studies using simultaneous scalp EEG recordings and fMRI during oddball tasks with respect to whether the BOLD signal and the P3b originate from the same neural generator. Many of these studies found concordant target-induced activation in the TPJ, as well as in other frontal and deep brain regions, including the middle frontal gyrus, thalamus, and insula (Menon et al. 1997; Horovitz et al. 2002; Mulert et al. 2004). In contrast, several studies report target-related P3b and BOLD signal activity in distinct regions. For instance, the P3b has been previously localized to the superior temporal gyrus (STG; Brázdil et al. 2005) and middle frontal gyrus (Mulert et al. 2004), but neither of these regions exhibited BOLD signal activity during target detection in their respective studies.

Using intracranial recordings with improved spatial resolution, our data indicate that the majority of electrodes showing target-specific HFB activity are distinct from those showing target-specific P3b responses. The predominant pattern of non-overlapping HFB and P3b electrodes indicates that these responses originate from different neural generators and that

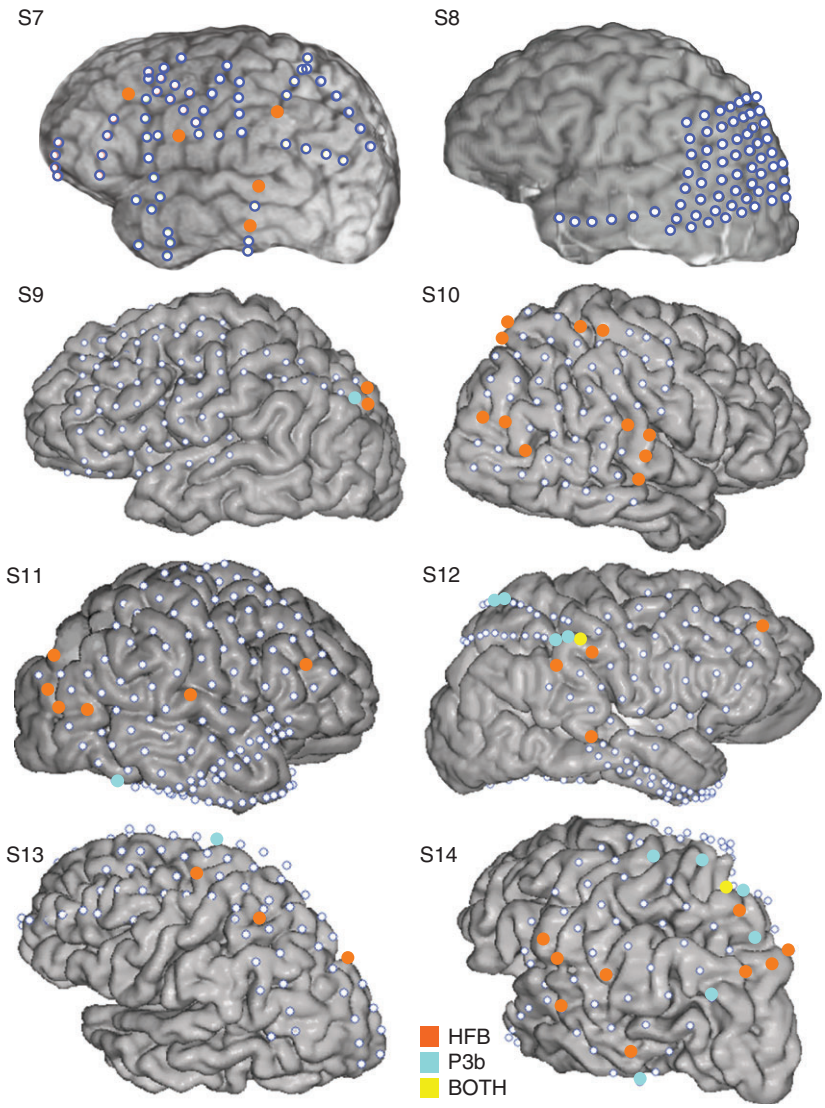

Figure 5. Locations of HFB and P3bs in visual experiment. The location of electrodes showing target-specific HFB (orange-colored markers), P3b activity (cyan-colored markers), and those electrodes showing both (yellow-colored markers) are presented on each individual subject's brain for the visual experiment.

these generators are distributed across the cortex. This supports previous studies using intracranial recordings that have also noted spatial distinctions between cortical ERPs and HFB activity (Crone et al. 2001; Szczepanski et al. 2014).

Implication of Task Differences on P3b Characteristics

Differences between the auditory and visual tasks may have contributed to the characteristics and the locations of the electrodes showing the P3b response, as observed in Figure 3. The most obvious difference between the 2 data sets is task modality. Evidence from source localization and lesion studies suggests several neural sources for the auditory and visual P3b. Specifically, source localization studies have localized the auditory P3b mainly to the superior temporal gyrus (Rogers 1991; Tarkka et al. 1995; Opitz et al. 1999; Mulert et al. 2004), inferior parietal lobule (IPL) (Menon et al. 1997; Mulert et al. 2004), and the TPJ (Mulert et al. 2004). In comparison, the visual P3b is linked to parietal cortical locations, including the IPL (Bledowski et al. 2004), intraparietal sulcus, and superior parietal lobule (Moores et al. 2003; Bledowski et al. 2004). These source localization results are generally consistent with the brain lesion literature (Knight et al. 1989; Verleger et al. 1994; Knight 1997). Notably, although these results suggest multiple sources for the auditory (i.e., a more temporal–parietal component) and visual (i.e., a more superior parietal component) P3b, the 2 modalities seem to share a common source in the IPL/TPJ region. In the current study, we found P3b responses spread across parietal, temporal, occipital (for the visual task only), and even some frontal cortical locations in both the auditory and visual tasks. Our results are in line with previous intracranial studies that demonstrate widely spatially distributed auditory and visual P3b components (e.g., Smith et al. 1990; Baudena et al. 1995a).

The 2 data sets also differ considerably in task parameters and trial structure. Both the auditory and visual tasks required subjects to attend to stimuli and to respond to the appearance of a predefined target. However, the auditory tasks used a classic oddball paradigm, with relatively few target instances compared with nontargets, whereas the visual task was a cuing

paradigm, in which targets were more common than nontargets. These differences between tasks may have impacted the amplitude and latency of the P3b response reported for each data set. For instance, P3 amplitudes are inversely proportional to the a priori stimulus probability (Duncan-Johnson and Donchin 1977), while P3 latencies are shortened with higher a priori probability of stimulus appearance (Duncan-Johnson and Donchin 1982). The higher probability of targets in the visual task may account for the shorter peak latencies found on average for the visual P3b components than the auditory P3b components, as can be observed in Figure 3.

Differences in P3b Morphology

One noteworthy aspect regarding the current study is the diverse characteristics of the target-specific P3b components across electrodes and subjects. As observed in Figure 3, the electrodes showing significant target-specific effects have different morphologies and peak times. This diversity of cortical ERP morphologies has been reported in previous intracranial studies (e.g., Halgren et al. 1995a, 1995b). These findings contrast with the classic P3b observed on the scalp, which is generally characterized as a positive deflection with a peak around 300 ms maximal over parietal cortex (Donchin and Coles 1988; Linden 2005). What might explain this discrepancy? One possibility is that our objective measure of the P3b based on peak onset and conditional differences, typically used in scalp EEG studies, does not adequately capture the P3b at the cortical level. A second possibility is that the cortical P3b morphology is inherently diverse, but averaging across multiple sources results in the standard ERP observed at scalp level. One observation from our data is that when ERP waveforms from individual electrodes are included into the grand average across electrodes and across patients (as can be observed in Fig. 3, moving from the left panel toward the right panel), the diverse features of the individual electrodes eventually morph into the archetypal scalp-level P3b that is observed in the resulting grand average.

In the current study, the P3b observed over many posterior cortical sites indicates that spatial smoothing of a number of neural sources averages into the traditional scalp P3b (Donchin and Coles 1988; Linden 2005; Polich 2007). This proposal extends previous evidence from multiple methodologies by suggesting that although the temporo–parietal cortex is the principal P3b neural generator (Knight et al. 1989; Menon et al. 1997), other areas also contribute to the P3b (McCarthy et al. 1989; Smith et al. 1990; Baudena et al. 1995b; Halgren 1995a, 1995b). Our results, along with these previous intracranial studies, lend support to the notion that multiple brain areas participate in successful target detection.

Supplementary Material

Supplementary data is available at *Cerebral Cortex* online.

Funding

Natural Sciences and Engineering Research Council of Canada Postdoctoral Fellowship (to J.W.Y.K.); National Institutes of Health (grants 2R37RO1NS21135 to R.T.K., 1R01NS078396 to J.P., and 1R01NS40596 to N.E.C.); National Institute of Neurological Disorders and Stroke (K23 NS060993 to J.J.L.); and the Nielsen Corporation.

Notes

The authors would like to thank all the patients for their time and contribution, as well as Callum Dewar and James Lubell for their assistance with figure preparation. *Conflict of Interest*: None declared.

References

Anderer P, Pascual-Marqui RD, Semlitsch HV, Saletu B. 1998. Differential effects of normal aging on sources of standard N1, target N1 and target P300 auditory event-related brain potentials revealed by low resolution electromagnetic tomography (LORETA). Electroencephalogr Clin Neurophysiol. 108:160–174.

Ardekani BA, Choi SJ, Hossein-Zadeh GA, Porjesz B, Tanabe JL, Lim KO, Bilder R, Helpern JA, Begleiter H. 2002. Functional magnetic resonance imaging of brain activity in the visual oddball task. Brain Res Cogn Brain Res. 14:347–356.

Bansal AK, Madhavan R, Agam Y, Golby A, Madsen JR, Kreiman G. 2014. Neural dynamics underlying target detection in the human brain. J Neurosci. 34:3042–3055.

Baudena P, Halgren E, Heit G, Clarke JM. 1995a. Intracerebral potentials to rare target and distractor auditory and visual stimuli. III. Frontal cortex. Electroencephalogr Clin Neurophysiol. 94:251–264.

Baudena P, Halgren E, Heit G, Clarke JM. 1995b. Intracerebral potentials to rare target and distractor auditory and visual stimuli. III. Frontal cortex. Electroencephalogr Clin Neurophysiol. 94:251–264.

Benjamini Y, Hochberg Y. 1995. Controlling the false discovery rate: a practical and powerful approach to multiple testing. J R Stat Soc.. 57:289–300.

Bledowski C, Prvulovic D, Goebel R, Zanella FE, Linden DEJ. 2004. Attentional systems in target and distractor processing: a combined ERP and fMRI study. Neuroimage. 22:530–540.

Brázdil M, Dobšík M, Mikl M, Hluštík P, Daniel P, Pažourková M, Krupa P, Rektor I. 2005. Combined event-related fMRI and intracerebral ERP study of an auditory oddball task. Neuroimage. 26:285–293.

Bressler SL. 2002. Event-related potentials. In: Handbook of Brain Theory and Neural Networks. Cambridge (MA): MIT Press. p. 412–415.

Canolty RT, Soltani M, Dalal SS, Edwards E, Dronkers NF, Nagarajan SS, Kirsch HE, Barbaro NM, Knight RT. 2007. Spatiotemporal dynamics of word processing in the human brain. Front Neurosci. 1:185–196.

Cardin JA, Carlén M, Meletis K, Knoblich U, Zhang F, Deisseroth K, Tsai L-H, Moore CI. 2009. Driving fast-spiking cells induces gamma rhythm and controls sensory responses. Nature. 459:663–667.

Clarke JM, Halgren E, Chauvel P. 1999. Intracranial ERPs in humans during a lateralized visual oddball task: II. Temporal, parietal and frontal recordings. Clin Neurophysiol. 110: 1226–1244.

Corbetta M, Shulman GL. 2002. Control of goal-directed and stimulus-driven attention in the brain. Nat Rev Neurosci. 3: 201–215.

Crone N, Boatman D, Gordon B, Hao L. 2001. Induced electrocorticographic gamma activity during auditory perception. Clin Neurophysiol. 112:565–582.

Donchin E, Coles M. 1988. Is the P300 component a manifestation of context updating? Behav Brain Sci. 11:357–374.

Downar J, Crawley AP, Mikulis DJ, Davis KD. 2001. The effect of task relevance on the cortical response to changes in visual

and auditory stimuli: an event-related fMRI study. Neuroimage. 14:1256–1267.

Duncan-Johnson C, Donchin E. 1982. The P300 component of the event-related brain potential as an index of information processing. Biol Psychiatry. 14:1–52.

Duncan-Johnson CC, Donchin E. 1977. On quantifying surprise: the variation of event-related potentials with subjective probability. Psychophysiology. 14:456–467.

Engell AD, McCarthy G. 2011. The relationship of gamma oscillations and face-specific ERPs recorded subdurally from occipitotemporal cortex. Cereb Cortex. 21:1213–1221.

Flinker A, Chang EF, Kirsch HE, Barbaro NM, Crone NE, Knight RT. 2010. Single-trial speech suppression of auditory cortex activity in humans. J Neurosci. 30:16643–16650.

Fogelson N, Shah M, Scabini D, Knight RT. 2009. Prefrontal cortex is critical for contextual processing: evidence from brain lesions. Brain. 132:3002–3010.

Freeman WJ. 2000. Mesoscopic neurodynamics: from neuron to brain. J Physiol Paris. 94:303–322.

Halgren E, Baudena P, Clarke JM, Heit G, Ligeois C, Chauvel P, Musolino A. 1995a. Intracerebral potentials to rare target and distractor auditory and visual stimuli. I. Superior temporal plane and parietal lobe. Electroencephalogr Clin Neurophysiol. 94:191–220.

Halgren E, Baudena P, Clarke JM, Heit G, Marinkovic K, Devaux B, Vignal JP, Biraben A. 1995b. Intracerebral potentials to rare target and distractor auditory and visual stimuli: II. Medial, lateral and posterior temporal lobe. Electroencephalogr Clin Neurophysiol. 94:229–250.

Handy TC. 2004. Event-related potentials: a methods handbook. Cambridge (MA): MIT Press.

Horovitz SG, Skudlarski P, Gore JC. 2002. Correlations and dissociations between BOLD signal and P300 amplitude in an auditory oddball task: a parametric approach to combining fMRI and ERP. Magn Reson Imaging. 20:319–325.

Keller CJ, Chen C, Lado FA, Khodakhah K. 2016. The limited utility of multiunit data in differentiating neuronal population activity. PLoS One. 11:e0153154.

Knight RT. 1997. Distributed cortical network for visual attention. J Cogn Neurosci. 9:75–91.

Knight RT, Scabini D, Woods DL, Clayworth CC. 1989. Contributions of temporal-parietal junction to the human auditory P3. Brain Res. 502:109–116.

Linden DE, Prvulovic D, Formisano E, Vollinger M, Zanella FE, Goebel R, Dierks T. 1999. The functional neuroanatomy of target detection: an fMRI study of visual and auditory oddball tasks. Cereb Cortex. 9:815–823.

Linden DE. 2005. The P300: where in the brain is it produced and what does it tell us? Neuroscientist. 11:563–576.

Logothetis NK, Pauls J, Augath M, Trinath T, Oeltermann A. 2001. Neurophysiological investigation of the basis of the fMRI signal. Nature. 412:150–157.

Luck SJ. 2005. An introduction to the event-related potential technique. Cambridge (MA): MIT Press.

Maris E, Oostenveld R. 2007. Nonparametric statistical testing of EEG- and MEG-data. J Neurosci Methods. 164:177–190.

McCarthy G, Wood CC. 1987. Intracranial recordings of endogenous ERPs in humans. Clin Neurophysiol. 39:331–337.

McCarthy G, Wood CC, Williamson PD, Spencer DD. 1989. Task-dependent field potentials in human hippocampal formation. J Neurosci. 9:4253–4268.

Mecklinger A, Ullsperger P. 1995. The P300 to novel and target events: a spatio- temporal dipole model analysis. Neuroreport. 7:241–245.

Menon V, Ford JM, Lim KO, Glover GH, Pfefferbaum A. 1997. Combined event-related fMRI and EEG evidence for temporal-parietal cortex activation during target detection. Neuroreport. 8:3029–3037.

Miller KJ. 2010. Broadband spectral change: evidence for a macroscale correlate of population firing rate? J Neurosci. 30:6477–6479.

Moores KA, Clark CR, Hadfield JLM, Brown GC, Taylor DJ, Fitzgibbon SP, Lewis AC, Weber DL, Greenblatt R. 2003. Investigating the generators of the scalp recorded visuoverbal P300 using cortically constrained source localization. Hum Brain Mapp. 18:53–77.

Muggleton NG, Cowey A, Walsh V. 2008. The role of the angular gyrus in visual conjunction search investigated using signal detection analysis and transcranial magnetic stimulation. Neuropsychologia. 46:2198–2202.

Mulert C, Jäger L, Schmitt R, Bussfeld P, Pogarell O, Möller HJ, Juckel G, Hegerl U. 2004. Integration of fMRI and simultaneous EEG: Towards a comprehensive understanding of localization and time-course of brain activity in target detection. Neuroimage. 22:83–94.

Nir Y, Fisch L, Mukamel R, Gelbard-Sagiv H, Arieli A, Fried I, Malach R. 2007. Coupling between neuronal firing rate, gamma LFP, and BOLD fMRI is related to interneuronal correlations. Curr Biol. 17:1275–1285.

Nourski K V, Steinschneider M, Oya H, Kawasaki H, Howard MA. 2014. Modulation of response patterns in human auditory cortex during a target detection task: an intracranial electrophysiology study. Int J Psychophysiol. 95:191–201.

Opitz B, Mecklinger A, Von Cramon DY, Kruggel F. 1999. Combining electrophysiological and hemodynamic measures of the auditory oddball. Psychophysiology. 36: 142–147.

Polich J. 2007. Updating P300: an integrative theory of P3a and P3b. Clin Neurophysiol. 118:2128–2148.

Polich J, Herbst KL. 2000. P300 as a clinical assay: rationale, evaluation, and findings. Int J Psychophysiol. 38:3–19.

Pritchard WS. 1981. Psychophysiology of P300. Psychol Bull. 89: 506–540.

Ray S, Maunsell JH. 2011. Different origins of gamma rhythm and high-gamma activity in macaque visual cortex. PLoS Biol. 9(4):e1000610.

Rogers RL. 1991. Localization of the P3 sources using magnetoencephalography and magnetic resonance imaging. Clin Neurophysiol. 79:308–321.

Smith ME, Halgren E, Sokolik M, Baudena P, Musolino A, Liegois-Chauvel C, Chauvel P. 1990. The intracranial topography of the P3 event-related potential elicited during auditory oddball. Electroencephalogr Clin Neurophysiol. 76: 235–248.

Sutton S, Braren M, Zubin J, John ER. 1965. Evoked-potential correlates of stimulus uncertainty. Science. 150:1187–1188.

Szczepanski SM, Crone NE, Kuperman RA, Auguste KI, Parvizi J, Knight RT. 2014. Dynamic changes in phase-amplitude coupling facilitate spatial attention control in fronto-parietal cortex. PLoS Biol. 12:e1001936.

Tarkka IM, Stokic DS, Basile LFH, Papanicolaou AC. 1995. Electric source localization of the auditory P300 agrees with magnetic source localization. Clin Neurophysiol. 75:275–287.

Verleger R, Heide W, Butt C, Kompf D. 1994. Reduction of P3b in patients with temporo-parietal lesions. Cogn Brain Res. 2: 103–116.

Wilcoxon F. 1945. Individual comparisons by ranking methods. Biometrics Bull. 6:80–83.